atmosphere

MDPI

Article

Land Cover Changes and Land Surface Temperature Dynamics in the Rohingya Refugee Area, Cox Bazar, Bangladesh: An Analysis from 2013 to 2024

Sourav Karmakar [1], Mizanur Rahman [2,3] and Lei Meng [2,*]

[1] Department of Geography, University of Tartu, Ülikooli tn 18, 50090 Tartu, Estonia
[2] School of Environment, Geography, and Sustainability, Western Michigan University, Kalamazoo, MI 49008, USA; mizanur.rahman@wmich.edu
[3] Little Rock Water Reclamation Authority, 11 Clearwater Dr, Little Rock, AR 72204, USA
* Correspondence: lei.meng@wmich.edu

Abstract: The rapid expansion of refugee settlements has caused significant environmental changes, particularly in regions experiencing forced displacement. The Rohingya refugee crisis in Cox's Bazar, Bangladesh, has led to extensive deforestation and land transformation, affecting local climate conditions. While urbanization's impact on land surface temperature (LST) is well-documented, the environmental consequences of unplanned refugee settlements remain understudied. This study investigates land cover changes and LST dynamics from 2013 to 2024, offering a novel perspective on refugee-induced environmental changes. Using Landsat 8 imagery, four key land cover categories (built-up, mixed forest, water bodies, and barren land) were classified through a Support Vector Machine (SVM) approach. The temporal change in these key land cover categories was examined. The surface temperature product (Band 10) from Landsat 8 Collection 2 Level 2 (C2 L2) was applied to derive LST, while Normalized Difference Vegetation Index (NDVI), Normalized Difference Water Index (NDWI), and Normalized Difference Built-up Index (NDBI) were used to assess vegetation and urbanization trends. Findings reveal a 97% decline in forest cover and a 161.78% increase in built-up areas between 2013 and 2018, leading to substantial LST increases. Statistical analyses confirm strong correlations between LST and multispectral indices, with vegetation and water bodies acting as cooling agents, while urban areas amplify heat stress. This study underscores the urgent need for sustainable land management and reforestation efforts to mitigate environmental degradation. It also highlights the importance of global cooperation in balancing humanitarian needs with environmental sustainability, providing insights for policymakers and urban planners to enhance climate resilience in vulnerable regions.

Keywords: land use; land surface temperature; refugee crisis; Cox's Bazar; environmental impact; NDVI; NDWI; NDBI; urban heat island

Received: 16 January 2025
Revised: 18 February 2025
Accepted: 21 February 2025
Published: 23 February 2025

Citation: Karmakar, S.; Rahman, M.; Meng, L. Land Cover Changes and Land Surface Temperature Dynamics in the Rohingya Refugee Area, Cox Bazar, Bangladesh: An Analysis from 2013 to 2024. *Atmosphere* **2025**, *16*, 250. https://doi.org/10.3390/atmos16030250

1. Introduction

The rapid transformation of land use and land cover (LULC) due to urbanization and forced migration has become a critical environmental issue globally [1]. These changes significantly impact land surface temperature (LST), contributing to climate-related challenges such as the urban heat island (UHI) effect. The UHI effect occurs when natural landscapes are replaced by impervious surfaces such as roads and buildings, reducing vegetation and increasing heat retention in urbanized areas [2]. This phenomenon has

been extensively studied in various regions, including urban areas in the United States, Europe, and Asia, where LULC changes have been directly linked to rising LST [3]. However, the environmental impact of forced displacement and unregulated land transformation in refugee settlements remains underexplored, particularly in rapidly developing or crisis-affected regions.

The Rohingya refugee influx into Cox's Bazar, Bangladesh, since 2017 represents a unique case of unplanned settlement expansion [4]. The forced displacement from Myanmar has resulted in one of the largest refugee settlements in the world, intensifying land-use pressure and causing severe ecological damage [5,6]. Bangladesh, already grappling with deforestation, air quality degradation, and industrial expansion, faces heightened environmental challenges due to the sudden population surge [7,8]. This crisis has accelerated forest depletion, loss of biodiversity, and soil erosion with long-term ecological and climatic consequences [9].

Previous studies have examined various environmental consequences of refugee settlements, including soil hydrology and erosion, deforestation, and climate change [9]. For instance, Hasan et al. found that evapotranspiration rates in refugee settlements decreased by 40% due to vegetation loss [10], disrupting natural energy exchanges and accelerating surface warming. Rahman et al. reported that nearly 21,000 acres of dense forest were lost within one year of refugee settlement expansion [6]. Hasan et al. also highlighted that approximately 4300 acres of forest were cleared to accommodate refugees, altering regional climate patterns [10].

The rapid transformation of natural landscapes into refugee settlements has disrupted the natural energy balance through vegetation loss and the expansion of impervious surfaces, leading to increased LST in the region [9,11]. While LST is not a direct measure of air temperature or thermal comfort, it is a key environmental indicator of surface warming. Kafy et al. projected that by 2041, 22.51% of Cox's Bazar may experience LST values exceeding 32 °C, underscoring the need for immediate reforestation and sustainable land management [12]. Ren et al. highlight that deforestation in Cox's Bazar has intensified the UHI effect, leading to higher temperatures due to increased impervious surfaces and vegetation loss [11]. Mahi et al. linked deforestation and impervious surface expansion to an increasing UHI effect in the greater Teknaf peninsula [13]. Bappa et al. focused on LST changes between 2015 and 2021 but concentrated only on the Kutupalong Refugee Camp [14].

A comprehensive, long-term analysis of LULC and LST changes within the refugee camp area remains unexplored. Understanding these dynamics over an extended period is crucial for assessing the cumulative effects of forced displacement on climate regulation and ecosystem stability. This study aims to bridge this gap by comprehensively analyzing LULC and LST dynamics over a 10-year period, focusing on how the Rohingya refugee influx has influenced land cover changes and temperature variations. It hypothesizes that refugee-induced deforestation and urban expansion have led to significant thermal stress in Cox's Bazar, contributing to a persistent increase in LST, particularly in built-up areas. By investigating LST dynamics associated with four key land cover (LC) categories—built-up, mixed forest, water bodies, and barren land—alongside their interaction with the Normalized Difference Vegetation Index (NDVI), Normalized Difference Water Index (NDWI), and Normalized Difference Built-up Index (NDBI), this research seeks to provide insights into the environmental consequences of large-scale forced displacement and contribute to evidence-based decision-making for sustainable land management.

2. Study Area, Dataset, and Methods

2.1. Study Area

The study area (Figure 1) is in the southern part of Bangladesh, encompassing two Upazilas (sub-districts) within the coordinates 20°43′0″ N to 21°18′0″ N latitude and 92°4′0″ E to 92°20′0″ E longitude. This region contains 34 refugee camps, which are the focal points for the analysis. The outline boundary data for the study area were obtained from the Humanitarian Data Exchange platform (data.humdata.org). The area is situated within a subtropical monsoon climate zone, characterized by three distinct seasons: winter (October–March), summer (March–June), and the rainy season (June–October). The region has an average monthly temperature of 25.90 °C and an annual average precipitation of approximately 4068 mm/year from 1975 to 2016.

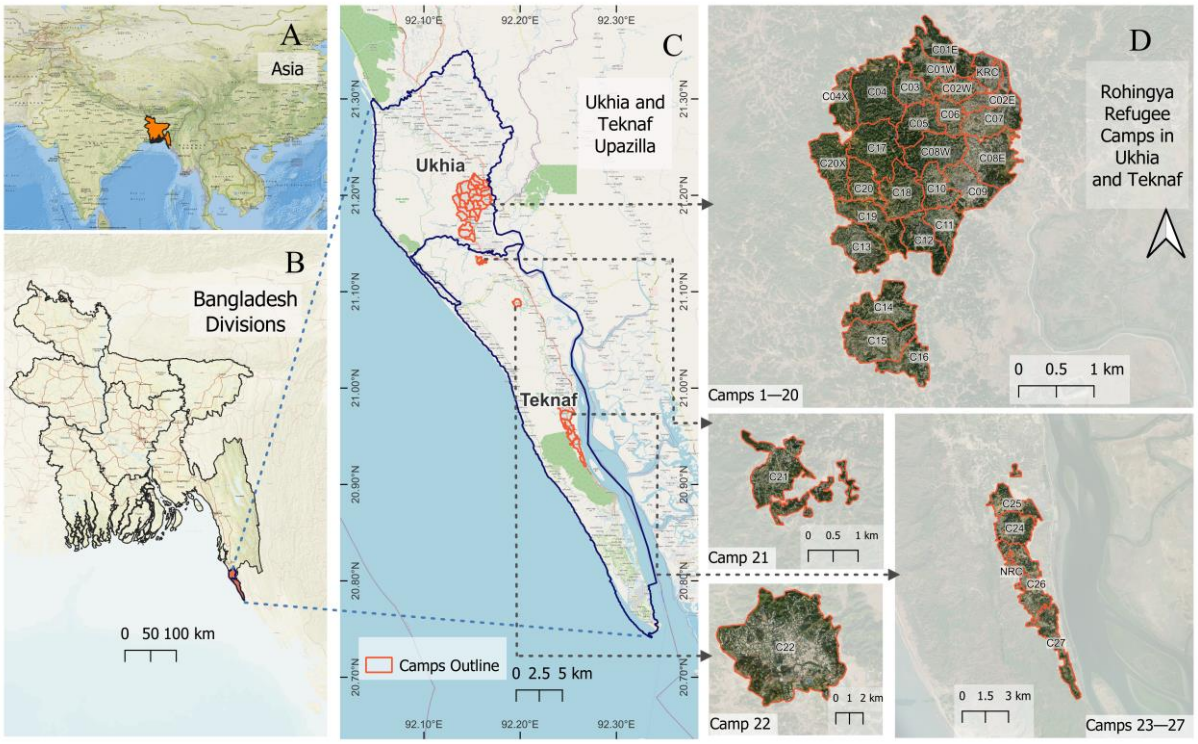

Figure 1. Study area map: (**A**). Esri national geographic base map centered in Asia, (**B**). Bangladesh Administrative boundary (Basemap: Esri Standard), (**C**). Ukhia and Teknaf Upazilla of Cox's Bazar district (Basemap: Open-street Map), and (**D**). Rohingya refugee camps (Basemap: Bing virtual earth).

The 34 refugee camps in this region are home to over one million refugees. Camp 15, the largest population, hosted approximately 49,468 refugees at the time of the study. Nayapara RC, the second largest and one of the oldest camps, housed around 37,000 refugees. Camp 20 (extension), located north of Camp 15, is the smallest, with an estimated population of 4630 refugees, according to UNCHR [2].

Hills and natural forests dominate the physiography of the area. Located near the Bay of Bengal, this salinity-prone region is poorly suited for agriculture [3]. It is home to several endangered species, including shoreline, offshore birds, and the wild Asian elephant [4]. However, establishing refugee camps and related anthropogenic activities have degraded the region's lush greenery and biodiversity [15].

2.2. Satellite Data Processing

This study used Landsat 8 satellite imagery with a 30 m ground resolution due to the availability of thermal infrared bands. The imagery was sourced from the U.S. Geological

Survey's (USGS) Landsat 8 Collection 2, Tier 1 Level 2 dataset via the Google Earth Engine (GEE) platform, which provides atmospherically corrected surface reflectance (SR) and surface temperature (ST) data. Three study years, 2013, 2018, and 2024, were selected to assess pre-crisis, post-crisis, and recent trends in LST. For each year, imagery was filtered between 1 April and 31 August and limited to the region of interest to ensure spatial consistency (see Table A1). Landsat images with less than 20% cloud cover were sorted within the study period. Then, a cloud mask was applied using the quality assurance band (QA_PIXEL band), where bitwise operations exclude pixels affected by clouds or shadows. Optical and thermal bands were calibrated using standard scaling factors described in the metadata. Satellite datasets used in this study were projected to WGS 84/UTM zone 46N. To maintain consistency, the same pre-processed images were used for the LST retrieval, land cover classification, and indices calculation.

2.3. Retrieval of LST from Landsat Data

Land surface temperature (LST) retrieval from satellite images has traditionally required multiple processing steps, including atmospheric corrections, emissivity estimations, and radiative transfer models. Previously, methods such as the mono-window algorithm (MWA), the split window algorithm (SWA), and the single-channel (SC) algorithm were commonly used to retrieve LST from Landsat bands [16,17]. These methods involved calculating brightness temperature from Top-of-Atmosphere (TOA) radiance, estimating emissivity using vegetation indices, and applying correction factors to derive LST. However, with advancements in remote sensing, Landsat 8 Collection 2 Level 2 (C2 L2) now provides a pre-processed surface temperature (ST) product, eliminating the need for user-applied atmospheric corrections and simplifying LST extraction. The C2 L2 ST product, available from April 2014, is derived using a single-channel algorithm applied to the Thermal Infrared Sensor (TIRS) band 10. It incorporates TOA reflectance, TOA brightness temperature, land surface emissivity from the Advanced Spaceborne Thermal Emission and Reflection Radiometer (ASTER) Global Emissivity Dataset (GED), and atmospheric corrections based on reanalysis data [18]. This study used analysis-ready data from Landsat 8 C2 L2 collection available in GEE. We used the standardized scaling factor and offset level described in the metadata and subtracted 273 to convert the LST unit from Kelvin to degree Celsius.

2.4. Land Use and Land Cover Classification

Landsat imagery was classified into four LC types: built-up, barren land, mixed forest, and water bodies. The Support Vector Machine (SVM) supervised classification method in ArcGIS Pro was employed due to its effectiveness in heterogeneous landscapes with limited training samples [19,20]. This classification produced land cover maps, enabling an analysis of land cover changes from 2013 to 2024 to assess environmental and land use dynamics. The accuracy of the classified maps is assessed using 150 random sample ground truth data from Google Earth Pro. Several accuracy metrics, such as Overall Accuracy, User Accuracy, Producer Accuracy, and Kappa Statistics, are calculated based on Equations (1)–(4). These metrics provided a comprehensive assessment, validating the effectiveness of the classification approach [21].

$$\text{Overall Accuracy} = \frac{\sum \text{diag(C)}}{\text{N}} \times 100 \quad (1)$$

$$\text{User Accuracy} = \frac{C_{ii}}{\sum C_{ir}} \times 100 \quad (2)$$

$$\text{Producer Accuracy} = \frac{C_{ii}}{\sum C_{ri}} \times 100 \quad (3)$$

$$\text{Kappa Coefficient} = \frac{N\sum \text{diag(C)} - \sum(C_{ri} \times C_{ir})}{N^2 - \sum(C_{ri} \times C_{ir})} \times 100 \quad (4)$$

where C = confusion matrix, ∑diag (C) = sum of the diagonal elements (correctly classified pixels), N = total number of reference pixels, C_{ii} = number of correctly classified pixels for class i, $\sum C_{ir}$ = total number of reference pixels in row i (row total), $\sum C_{ri}$ = total number of reference pixels in column i (column total), C_{ri} = column total for class i, and C_{ir} = row total for class i.

User Accuracy measures commission errors and indicates the likelihood that a pixel is correctly identified. Higher values show fewer false positives and more accurate classification. Producer Accuracy assesses how well a ground-truth class is represented on the map, with higher values indicating fewer exclusions and better accuracy. The Overall Accuracy calculates the ratio of correctly classified pixels to the total number, providing a straightforward percentage of classification accuracy. The Kappa Statistics accounts for chance agreement, offering a detailed assessment of classification reliability. Values above 0.8 typically indicate a high level of agreement beyond random chance.

2.5. Indices Used in This Study

Multispectral indices derived from satellite imagery are widely used to analyze land cover characteristics, as they enhance the ability to extract information about vegetation, water bodies, and built-up areas by leveraging spectral reflectance properties [22,23]. These indices provide insights into surface biophysical conditions, enabling the assessment of environmental changes and their impact on LST [22,24]. In this study, we calculated the NDVI, NDWI, and NDBI according to the formula described in Table 1 to examine how vegetation patterns, water bodies, and built-up areas influence LST. NDVI is an indicator of surface emissivity and surface energy balance, impacting LST [25]. We used NDVI to assess the decline of green spaces due to the establishment of refugee camps and its effect on LST. NDWI is another widely used index to evaluate the presence of water bodies and moisture contents. While higher NDWI values are often associated with lower surface temperature due to the cooling effect of water bodies [26], the relationship between NDWI and LST can vary depending on local environmental factors [27]. On the other hand, the NDBI index is commonly used to detect urban areas, and it has a close relationship with LST as built-up regions provide the impervious surface, impacting surface emissivity and reflectance [28,29]. We calculated NDBI to understand how urbanization due to refugee settlement leads to higher LST. Integrating these multispectral indices with LST analysis allows for a detailed investigation of land cover changes and their influence on local thermal environments, which is further analyzed statistically in the following section.

Table 1. Multispectral indices used in this study, their associated bands for Landsat 8, and the references.

Indices	Bands	Formula	Reference
NDVI	$\frac{\text{Band5}-\text{Band4}}{\text{Band5}+\text{Band4}}$	$\frac{\text{NIR}-\text{Red}}{\text{NIR}+\text{Red}}$	Tucker [30]
NDWI	$\frac{\text{Band3}-\text{Band5}}{\text{Band3}+\text{Band5}}$	$\frac{\text{Green}-\text{NIR}}{\text{Green}+\text{NIR}}$	McFeeters [31]
NDBI	$\frac{\text{Band6}-\text{Band5}}{\text{Band6}+\text{Band5}}$	$\frac{\text{SWIR}-\text{NIR}}{\text{SWIR}+\text{NIR}}$	Zha et al. [32]

2.6. Statistical Analysis

This study employed a combination of statistical analyses to examine the relationship between land cover changes and LST dynamics in the Rohingya refugee area from 2013 to 2024. Descriptive statistics were used to summarize key characteristics of land cover categories and LST variations. A one-way Analysis of Variance (ANOVA) was conducted

to assess whether significant differences existed in LST across land cover types. Post hoc pairwise comparisons using the Scheffé test were applied to further investigate specific differences among land cover categories. Additionally, linear regression analysis was utilized to quantify the relationship between LST and land cover indices. The data used for linear regression analysis included satellite-derived land cover indices (NDVI, NDWI, and NDBI) and corresponding LST values for 2013, 2018, and 2024. These statistical approaches provided a comprehensive understanding of the impact of land cover changes on surface temperature dynamics in the study area.

3. Results

3.1. Land Use and Land Cover Changes from 2013 to 2024

Figure 2 reveals significant land cover changes from 2013 to 2024 in the study area across four primary classes- Built-up, barren land, mixed forest, and water bodies. According to our analysis, the built-up area expanded drastically to 161.78%, growing from 808.25 hectares in 2013 to 2115.85 hectares in 2018 (Table 2). This extensive growth indicates the rapid establishment of refugee settlements and infrastructural development to accommodate this huge Rohingya refugee population. However, urban areas slightly decreased by 7.43% from 2018 to 2024. This trend indicates positive efforts in the study area, such as alternative land-use practices that mitigate environmental stress. This study found that water bodies decreased from 15.22 hectares to only 0.45 hectares from 2013 to 2018, a 97.04% reduction. Large-scale modifications, like water body removal to create enough space for settlement, are the major cause of this significant change. Surprisingly, water bodies rebounded by 2220% and increased to 10.44 hectares. Establishing artificial ponds and water conservation initiatives to ensure water availability in the camp has contributed to this expansion [33]. Table 2 shows that from 2013 to 2018, barren land decreased by 19.79%, shrinking from 256.21 hectares to 205.51 hectares due to the conversion into residential areas. But after 2018, it expanded by 63.76% and reached 336.54 hectares in 2024 (Table 2). Deforestation or clearing activities to meet the demands and support temporary land uses may have contributed to this transformation within camps.

Table 2. Areal distribution (in hectares) of different land cover classes in the study area.

Class Name	Area 2013 (ha)	Area 2018 (ha)	Area 2024 (ha)	Change (2013–2018) (%)	Change (2018–2024) (%)
Built-up	808.25	2115.85	1958.7	161.78%	−7.43%
Water bodies	15.22	0.45	10.44	−97.04%	2220.0%
Barren land	256.21	205.51	336.54	−19.79%	63.76%
Mixed forest	1279.41	37.28	53.4	−97.09%	43.24%

Our research findings show that the mixed forest category experienced a sharp drop from 1279.41 hectares to just 37.28 hectares (Table 2) between 2013 and 2018, a 97.09% reduction. It likely resulted from land clearing for the refugee settlement. Moreover, due to reforestation or afforestation, the mixed forest area slightly increased to 53.4 hectares, which is 43.24% in 2024.

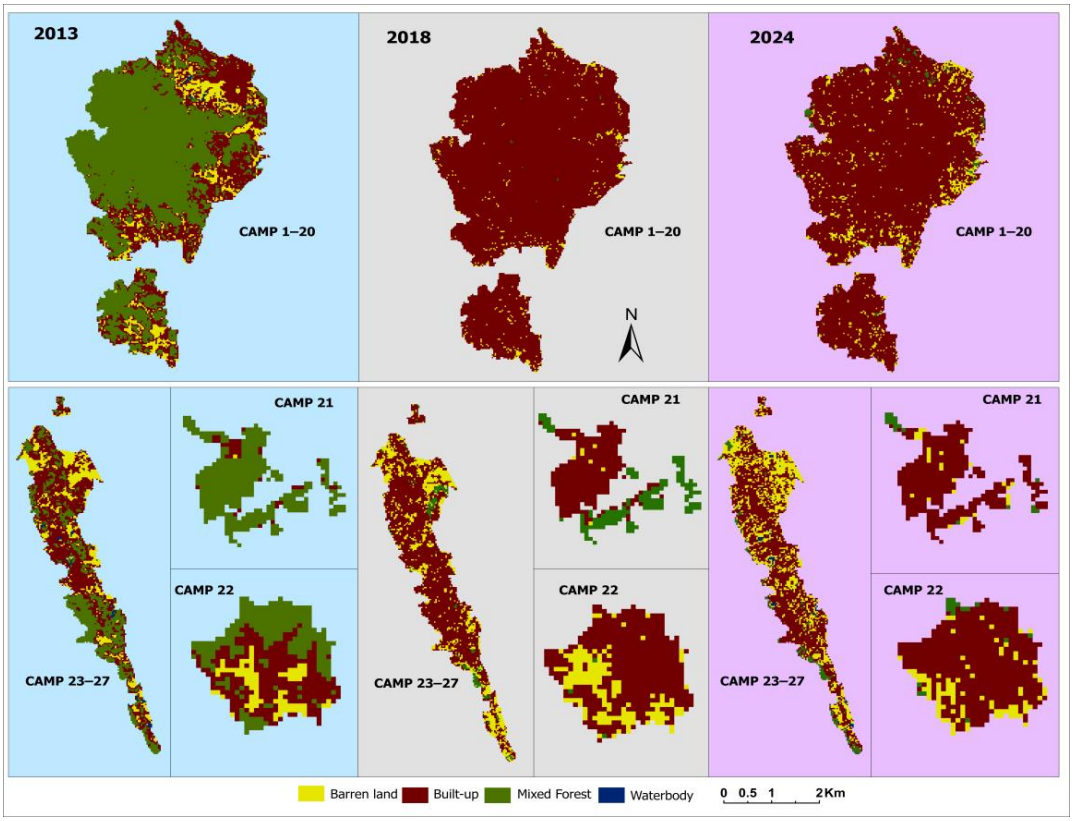

Figure 2. Land cover maps in 2013, 2018, and 2024.

The accuracy assessment (Table 3) for the classified land cover maps, spanning 2013 to 2024, was conducted using User Accuracy, Producer Accuracy, Overall Accuracy, and Kappa Statistics. The User Accuracy across land cover types—built-up, water bodies, barren land, and mixed forest—ranged from 80.00% to 94.59%, indicating the reliability of each classified class for end-users within the study area (Table 3). Producer Accuracy, which measures the ability of the classification to capture true positives for each class, ranged from 82.35% to 96.63% across these categories. The Overall Accuracy, calculated for 2013, 2018, and 2024, demonstrated a steady improvement, reaching 90.44% in 2024, while Kappa Statistics values increased from 0.849 to 0.875 (Table 3), confirming substantial agreement between the classification and reference data over time. These accuracy measures collectively validate the robustness and reliability of the classification approach used in this study.

Table 3. Accuracy assessment of supervised classification.

User Accuracy (%)				
LC class	Built-up	Water bodies	Barren land	Mixed forest
Year	2013–2024	2013–2024	2013–2024	2013–2024
Camps	88.00–92.00	80.00–94.59	84.00–94.33	87.50–92.00
Producer Accuracy (%)				
Camps	84.38–85.71	88.89–96.63	82.35–92.59	88.46–90.32
Overall Accuracy (%)				
Year	2013	2018	2024	
Camps	88.89	88.86	90.44	
Kappa Statistics (value from 0–1)				
Camps	0.849	0.853	0.875	

3.2. Land Surface Temperature Changes

Figures 3 and 4A indicate that our study area experienced an upward trend of LST from 2013 to 2024. In 2013, around 56% of the area (1493.46 ha) fell within the surface temperature range between 30.5 and 33.5 °C in 2013 (Figure 3 and Table A2). By 2018, more than 41% of the area experienced temperatures within 36.5–39.5 °C, while around 40% of the area experienced temperatures above 39.5 °C, possibly due to the massive influx of refugees' settlements within a very short period and a decrease in vegetation cover (Table A2). However, in 2024, temperature reduced slightly compared to 2018, where 44% of the area (1187 ha) experienced 33.5–36.5 °C, with 11% of the area still having temperatures more than 39.5 °C (Figure 4A). Our analysis also suggests that areas with the coolest temperature zone (<30.5 °C) decreased from 41 hectares to only 4 hectares from 2013 to 2024 (Figure 4A). In contrast, higher temperature zones expanded over the years, and most of the areas within refugee camps are in 33.5–39.5 °C temperature zones, which demonstrates increased thermal stress due to anthropogenic influences.

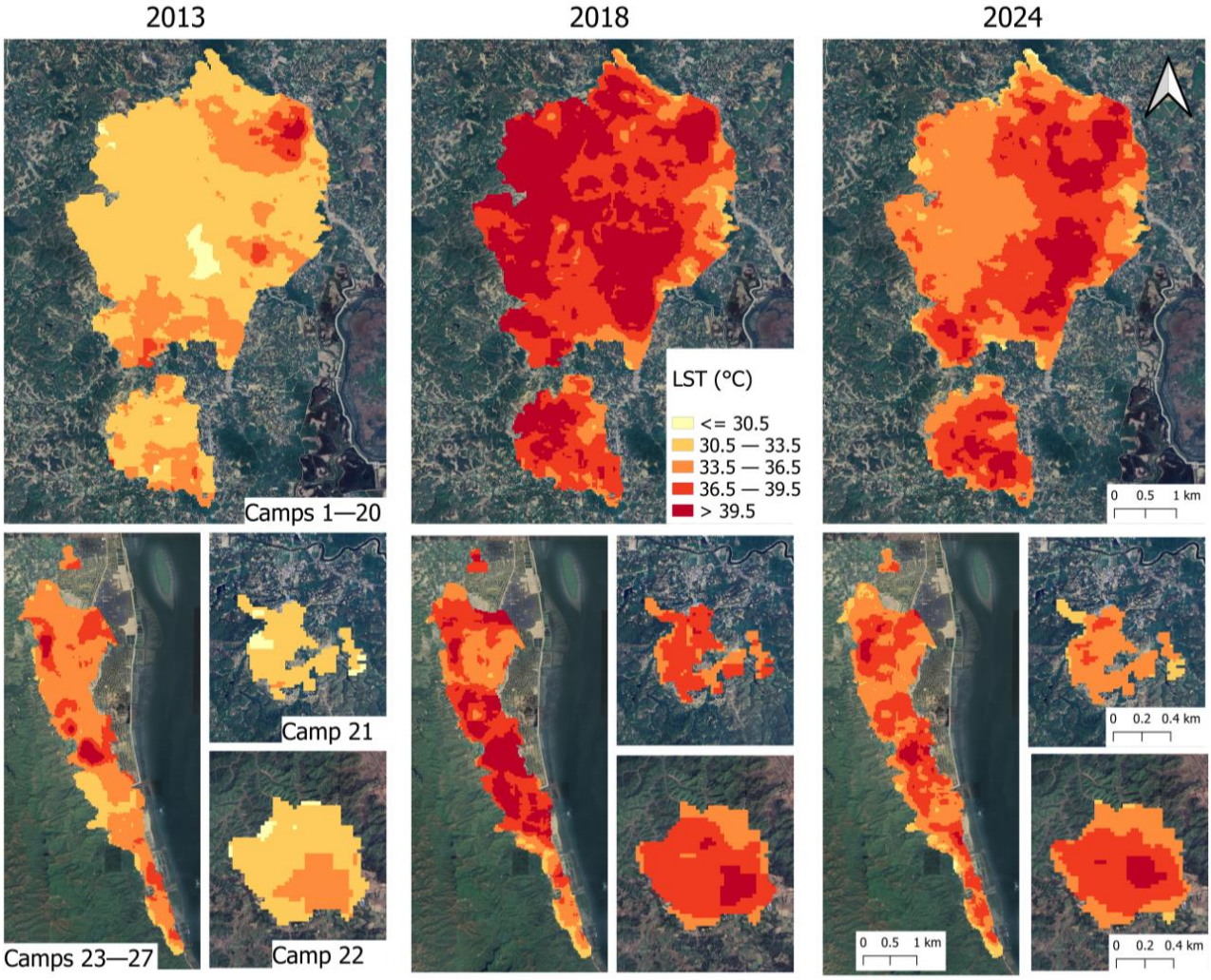

Figure 3. LST distribution maps for selected refugee camps in southern Bangladesh across 2013, 2018, and 2024. The color gradient represents LST in °C, with warmer colors indicating higher temperatures.

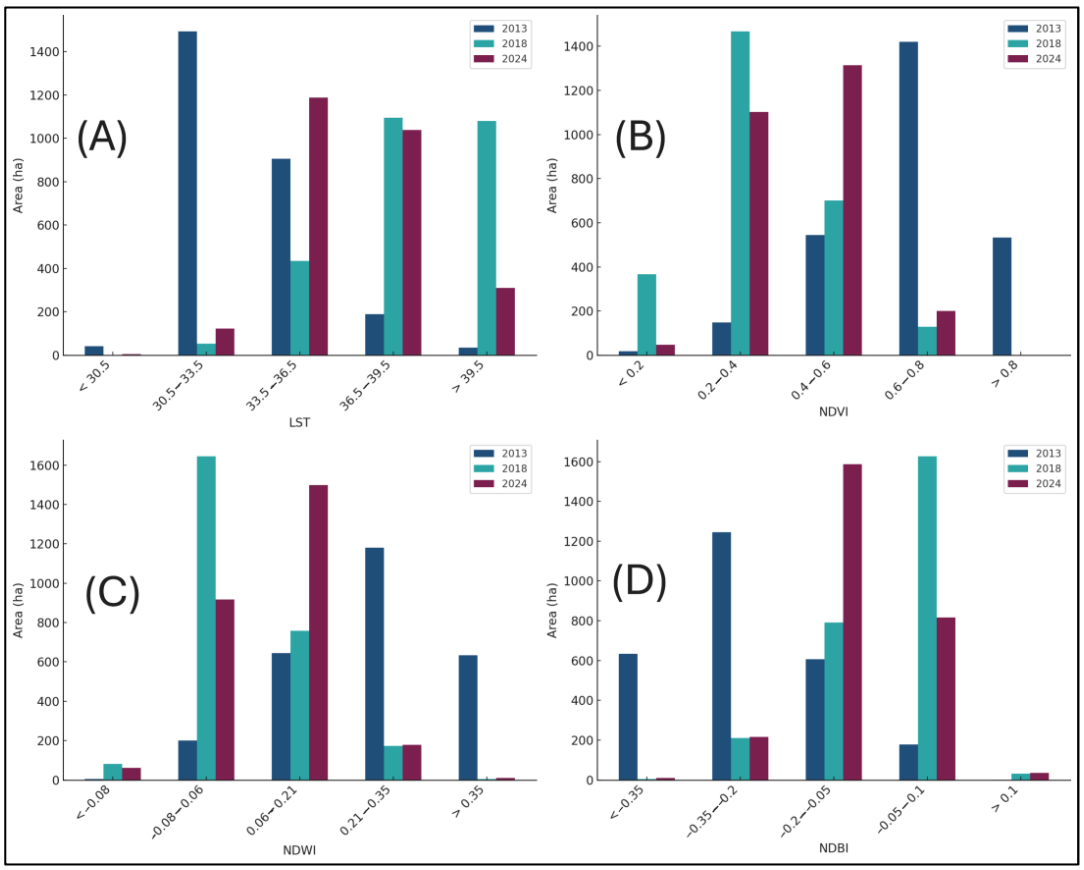

Figure 4. Calculated areas for different index ranges, presented in hectares (ha): (**A**) LST, (**B**) NDVI, (**C**) NDWI, and (**D**) NDBI.

3.3. Land Surface Temperatures and Land Cover Indices

There have been notable changes in NDVI across the study area from 2013 to 2024 (Figure 5). According to Figure 4B and Table A2, high NDVI values (0.6–0.8) occupied approximately 53.3% of the area in 2013, which indicates dense vegetation cover. However, by 2018, there was a sharp decrease in densely vegetated areas as indicated by NDVI (0.6–0.8), with a corresponding increase in areas classified under low-density vegetation areas with NDVI values less than 0.4 (Figure 4B and Table A2). Particularly, the area with NDVI value ranged from 0.2 to 0.4, which expanded from 5.58% in 2013 to 55.09% in 2018, according to Table A2.

By 2024, vegetation health improved moderately, as the area with NDVI from 0.4–0.6 covered nearly half the area (49.35%), although high-density vegetation with NDVI from 0.6–0.8 remained low at 7.51% (Figure 4B and Table A2). The area with very low vegetation cover (NDVI < 0.2) showed a fluctuating trend, peaking at 13.78% in 2018 and decreasing to 1.75% in 2024 (Figure 4B and Table A2). These changes indicate significant vegetation loss likely linked to anthropogenic pressures around the camps, with some recovery in later years due to plantation activity by several NGOs [34]. This emphasizes the need for ongoing conservation efforts to support vegetation regrowth and stabilize the ecosystem.

The NDWI maps for 2013, 2018, and 2024 reveal significant spatiotemporal changes in water content and moisture levels in the Rohingya refugee camps in Cox's Bazar, Bangladesh (Figure 6). In 2013, around 1180 ha (44.30%) of the area fell within the 0.21–0.35 NDWI range, with 23.78% exceeding 0.35, reflecting pre-crisis environmental stability characterized by abundant water resources and vegetation moisture (Figure 4C and Table A2). These conditions, represented by darker tones on the maps, indicate a healthy hydrological balance before the refugee influx.

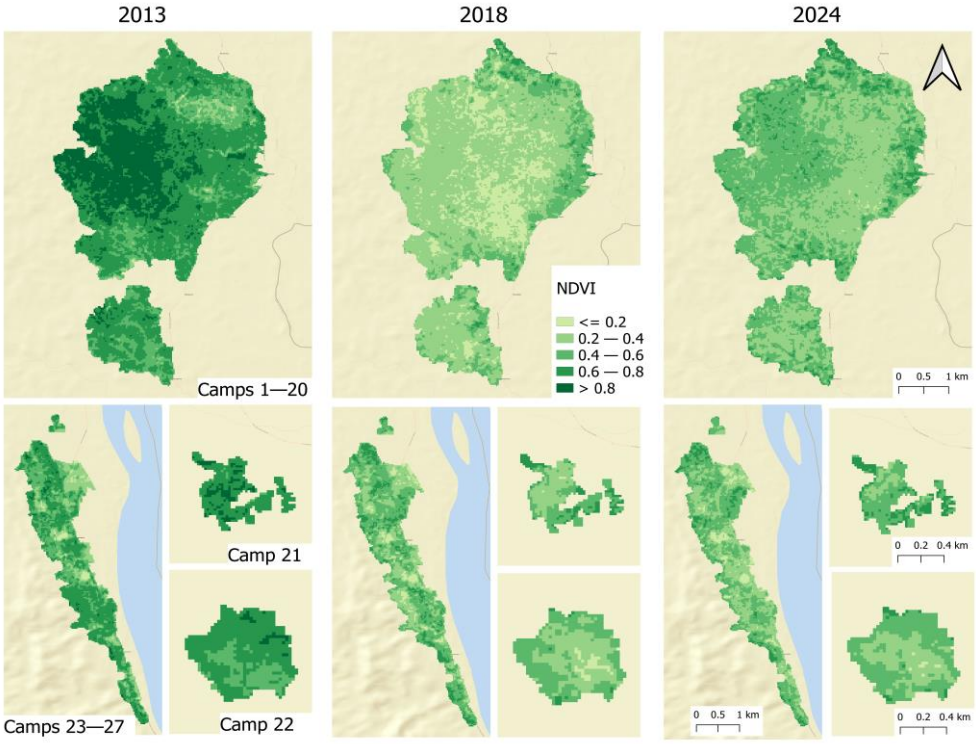

Figure 5. NDVI distribution maps for selected refugee camps across the years 2013, 2018, and 2024. The color gradient represents NDVI values, with darker colors indicating higher NDVI values (Basemap: ESRI standard).

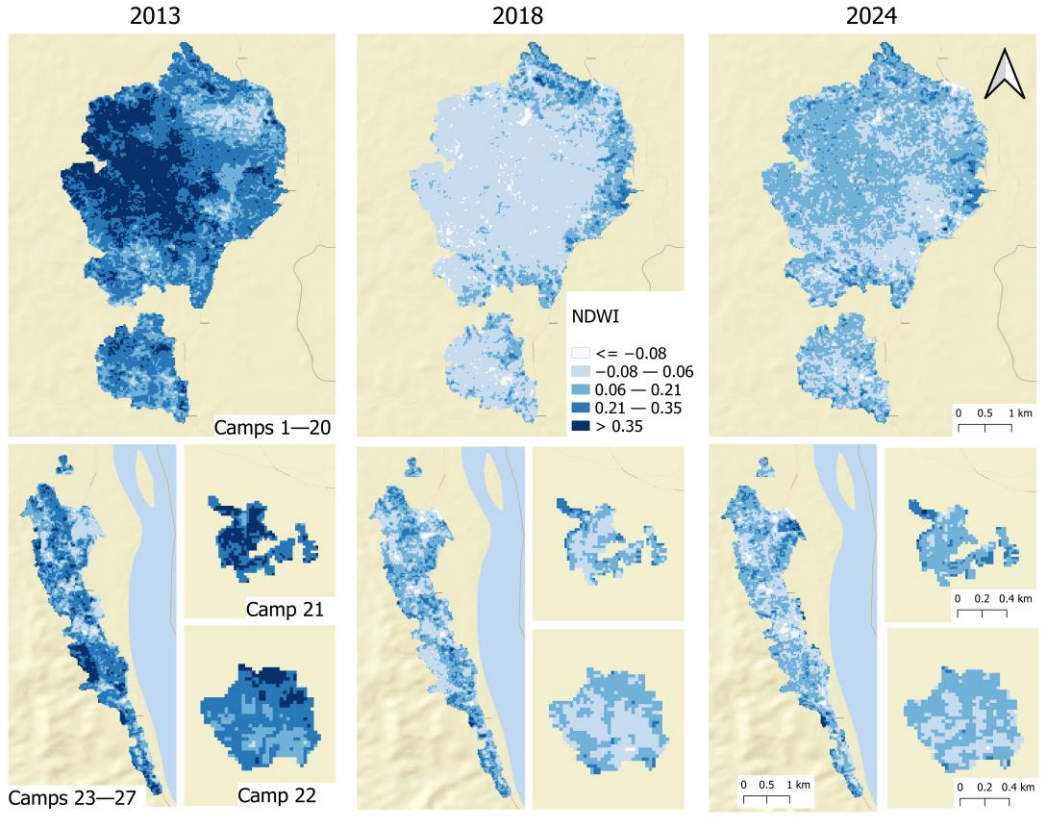

Figure 6. NDWI distribution maps for selected refugee camps across the years 2013, 2018, and 2024. The color gradient represents NDWI values, with darker colors indicating higher NDWI values (Basemap: ESRI standard).

By 2018, NDWI values showed a steep decline, with 61.78% of the area shifting to the −0.08–0.06 range and areas of high NDWI values (>0.35) dropping to 0.19% (Table A2). This degradation corresponds to extensive deforestation, land clearing, and soil compaction for refugee settlements, as human activities disrupt natural water retention. The lighter map tones highlight reduced moisture and declining surface water availability, consistent with environmental degradation observed in post-crisis studies (Figure 6).

In 2024, partial recovery is evident, with 56.27% of the area in the 0.06–0.21 NDWI range. However, an area with high NDWI values remains scarce, covering only 0.35% of the study region (Figure 4C and Table A2). The recovery may result from targeted reforestation and water management initiatives, although the limited restoration of water resources suggests the region's vulnerability to continued degradation.

The NDWI trends from 2013 to 2024 suggest the need for sustainable interventions to restore ecological balance. Enhanced water conservation practices and long-term environmental restoration are essential for mitigating the impacts of human activity on the region's hydrological system.

In 2013, the region exhibited relatively low NDBI values (Figure 7), with 46.74% of the area falling in the −0.35 to −0.20 range and only 0.07% exceeding 0.1. Correspondingly, most of the area experienced moderate LST values (30.5–33.5 °C) across 56% of the region (Figure 4A and Table A2). The increased built-up patterns in Figure 7 show less urbanization and stable thermal conditions in the pre-crisis environment. By 2018, rapid urbanization is evident, with moderately higher NDBI value (−0.05 to 0.1) increasing from 6% to 61%. Simultaneously, the LST range of 36.5–39.5 °C expanded to cover 41% of the area, with higher temperature zones (>39.5 °C) sharply increased (Figure 4A and Table A2). This demonstrates the impact of built-up infrastructure replacing natural vegetation, reducing evapotranspiration, and increasing heat absorption. In 2024, the trend persists, with 59.58% of the area falling into the −0.2 to −0.05 NDBI range, while LST values within 36.5–39.5 °C expanded to 23.08% (Table A2). These changes underscore the compounding effects of urbanization on temperature dynamics.

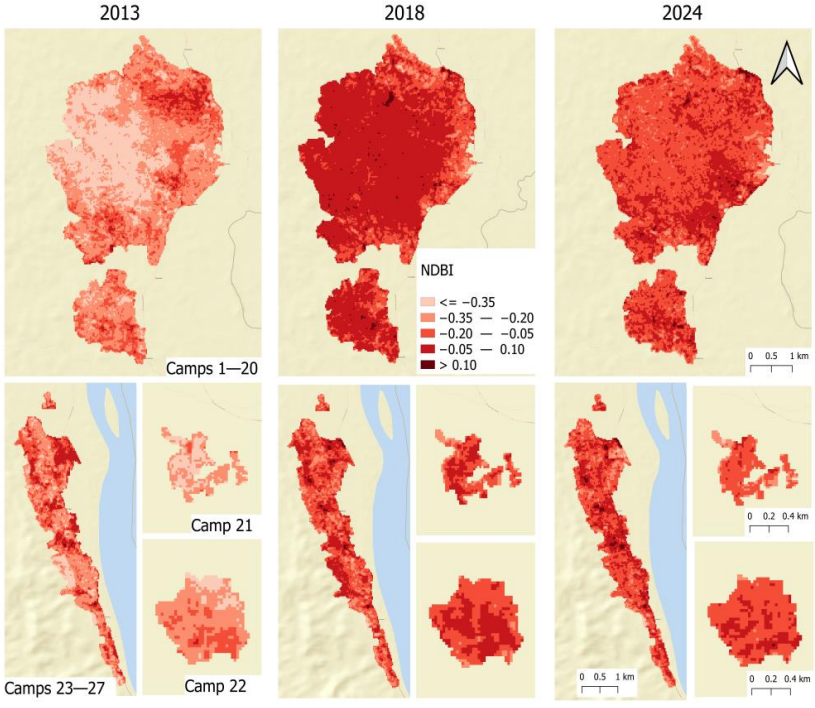

Figure 7. NDBI distribution maps for selected refugee camps across the years 2013, 2018, and 2024. The color gradient represents NDBI values, with darker colors indicating higher NDBI values (Basemap: ESRI standard).

3.4. Correlation Between LST and Land Cover Indices

The LST analysis across various land cover types comprehensively explains how vegetation, water content, and urbanization influence surface temperature dynamics. The findings, as summarized in Tables 4–6, demonstrate the significant role of land cover in moderating or amplifying surface temperatures within the study area.

Table 4. Post hoc pairwise comparison.

Multiple Comparisons (Scheffe)						
Dependent Variable: LST						
Categories	**Categories**	**Mean Difference**	**Std. Error**	**Sig.**	**95% Confidence Interval**	
					Lower Bound	**Upper Bound**
Mixed forest	Barren land	−2.34 *	0.21	<0.001	−2.93	−1.75
	Built-up	−2.48 *	0.19	<0.001	−3.01	−1.95
	Water bodies	−1.94 *	0.26	<0.001	−2.66	−1.22
Barren land	Built-up	−0.14	0.17	1	−0.60	0.32
	Water bodies	0.40	0.24	0	−0.27	1.07
Built-up	Water bodies	0.54	0.22	0	−0.08	1.16

*. The mean difference is significant at the 95% confidence level.

Table 5. Descriptive statistics of the four defined groups (mixed forest, barren land, built-up, and water bodies).

Descriptives (LST °C)								
	N	**Mean**	**Std. Deviation**	**Std. Error**	**95% Confidence Interval for Mean**		**Min**	**Max**
					Lower Bound	**Upper Bound**		
Mixed forest	160	31.61	1.78	0.143	31.33	31.89	26.89	36.44
Barren land	235	33.95	2.17	0.144	33.67	34.23	29.20	39.86
Built-up	440	34.09	2.08	0.098	33.90	34.28	28.78	40.38
Water bodies	105	33.55	1.86	0.182	33.19	33.91	29.10	37.99
Total	940	33.58	2.22	0.072	33.44	33.73	26.89	40.38

Table 6. Tests between and within the five defined groups for one-way ANOVA.

ANOVA (LST)					
	Sum of Squares	**df**	**Mean Square**	**F**	**Sig.**
Between Groups	855.41	3	285.13	70.34	<0.001
Within Groups	3794.20	936	4.05		
Total	4649.62	939			

The post hoc pairwise comparison (Table 4) reveals substantial differences in LST across land cover categories. Mixed forest areas consistently exhibit significantly lower LST than barren land, built-up areas, and water bodies, with mean differences of −2.34 °C, −2.48 °C, and −1.94 °C, respectively, which are all statistically significant at $p < 0.001$. This is further supported by the descriptive statistics (Table 5), which show that mixed forest areas have the lowest mean LST (31.61 °C), underscoring the critical role of vegetation in cooling the surface. The strong negative correlation between LST and NDVI (r = −0.62,

y = −7.207x + 36.866) in Figure 8A confirms this relationship. Vegetation reduces LST through shading and evapotranspiration, which lowers surface heating and improves thermal regulation. These findings align with broader studies on the cooling effects of vegetation, emphasizing the importance of preserving and enhancing forested areas in mitigating heat stress.

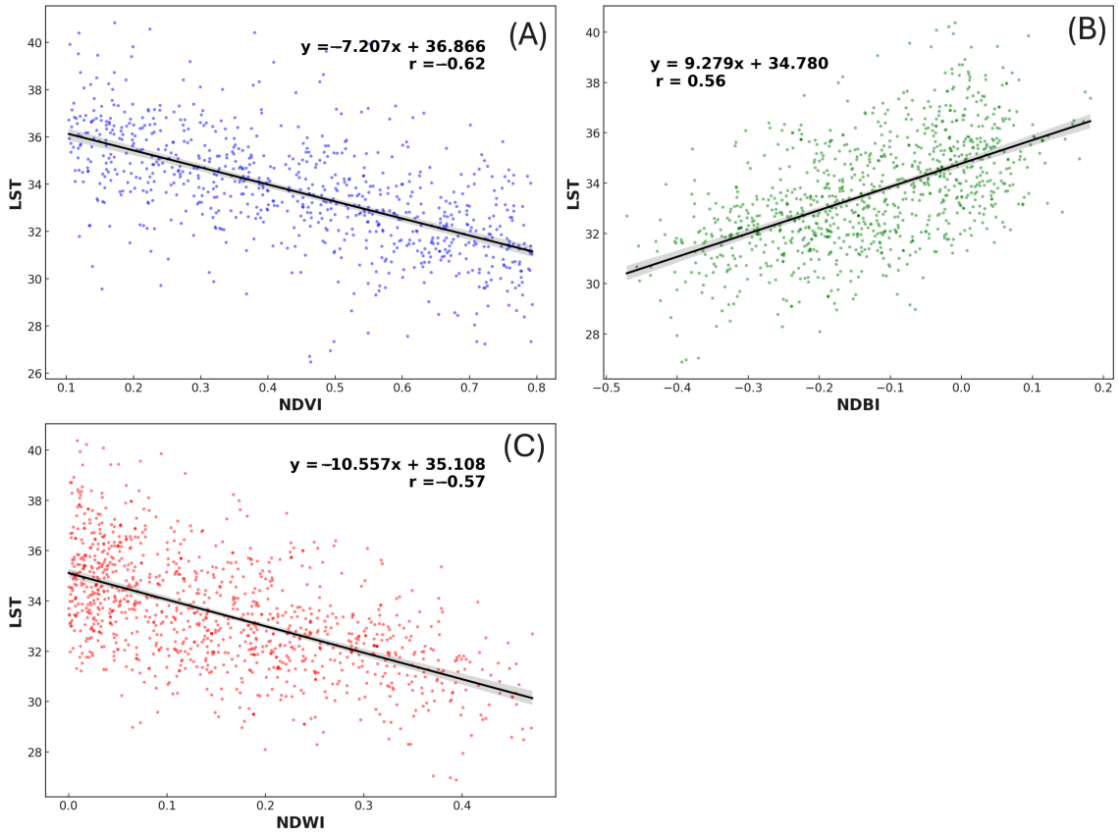

Figure 8. Correlations between LST (in degree Celsius) and (**A**) NDVI, (**B**) NDBI, and (**C**) NDWI aggregated for the years 2013, 2018, and 2024. All correlations are significant at the 95% confidence level.

Water bodies also demonstrate a cooling effect on LST, with a mean temperature of 33.55 °C (Table 5). The negative correlation between LST and NDWI (r = −0.57, y = −10.557x + 35.108) reflects the thermal properties of water, which absorbs and retains heat more efficiently than surrounding land cover types, leading to localized cooling (Figure 8C). However, water bodies exhibit slightly higher LST than mixed forest areas, potentially due to environmental factors such as evaporation rates and proximity to urbanized regions. Despite this, the role of water bodies in reducing LST remains significant, highlighting the importance of maintaining water resources in urban and semi-urban areas.

In contrast, built-up areas exhibit the highest mean LST (34.09 °C), as shown in Table 5. The positive correlation between LST and NDBI (r = 0.56, y = 9.279x + 34.780) confirms the urban heat island effect, where impervious surfaces such as concrete and asphalt absorb and radiate heat, leading to elevated temperatures in urbanized regions (Figure 8B). This relationship underscores the interconnected dynamics of urbanization and temperature changes in the Rohingya refugee camps from 2013 to 2024, where higher NDBI values correspond to elevated LST values. The ANOVA results (Table 6) further reinforce these findings, demonstrating significant differences in LST across land cover categories ($F = 70.34$, $p < 0.001$). Together, these results highlight the challenges associated with rapid development and the need for sustainable urban planning practices to reduce thermal stress.

The comparison of land cover types reveals a clear pattern: vegetation and water bodies act as natural cooling agents, while urbanized areas amplify surface temperatures. These insights emphasize the critical role of green and blue infrastructure in mitigating urban heat. Policies to increase vegetation cover, conserve water bodies, and reduce impervious surfaces can significantly enhance climate resilience and improve thermal comfort in urban and peri-urban settings. The statistical relationships detailed in Tables 4–6 provide robust evidence for integrating land cover management into urban planning to address the growing challenges of climate change and urbanization.

4. Discussion

This study highlights the significant environmental impact of the Rohingya refugee crisis on land cover transformation and land surface temperature (LST) dynamics in Cox's Bazar, Bangladesh. The analysis found that the area coverage with LST ranging from 36.5 °C to 39.5 °C expanded by 35% in 2018 and 32% in 2024 as compared to 2013. However, from 2018 to 2024, there was a slight 2% reduction in this temperature range due to the efforts from government, national and international NGOs. These findings align with similar trends observed in other studies within the region. For example, Bappa et al. reported a sixfold increase in average temperature between 2015 and 2018 [14]. Rashid et al. also documented a significant rise in LST from 2017 to 2019, with temperatures exceeding 31 °C in camp areas [35]. Hasan et al. observed maximum temperatures ranging from 20.29 °C to 35.89 °C across Teknaf, Ukhiya, Ramu, and Cox's Bazar in 2017, and similar results were also found by Ahmed et al., where they reported an increase in average temperature to 25.94 °C in 2022 when the average temperature was 18.86 °C to 21.31 °C from 1997 to 2017 [23,36]. Despite slight variations, these studies collectively confirm a consistent rise in LST in the refugee camps, correlating with extensive land cover changes.

Our study found a 97% reduction in forest cover and a 161.78% increase in built-up areas between the pre- and post-refugee crisis periods from 2013 to 2018. This is evidence of significant pressure on the forest clearing to make new homes for the refugees and the level of destruction by the refugees. These findings are consistent with other studies in Bangladesh and other parts of the world experiencing similar refugee influxes. Bappa et al. found that the Kutupalong Refugee Camp area experienced dramatic land use and land cover changes, with a 745% increase in settlements from 2015 to 2021, leading to the loss of 74% of forest cover and a rise in land surface temperature from 22.43 °C in 2015 to 30.22 degree Celsius in 2021, resulting in a temperature increase of 7.79 °C [14]. A comparison with similar crisis-induced environmental transformations globally reinforces the need for sustainable planning in refugee-hosting areas. For instance, studies on the Dadaab Refugee Camp in Kenya and the Zaatari Camp in Jordan reveal comparable patterns of vegetation loss, increased LST, and prolonged environmental degradation due to unplanned urbanization [5]. Rashid et al. documented a loss of 1876 hectares of forest between 2017 and 2021 in Kutupalong and Balukhali refugee camp, while Hasan et al. found an 80% reduction in forest area within the camp region, accompanied by a 6.16% decrease in vegetation cover along with temperature increase up to maximum 34 °C, which is significantly higher than the pre-influx period in the broader Cox's Bazar area [23,35]. These findings strongly suggest that the LST increase is associated with the large-scale reduction of forest cover and expansion of built-up areas following the establishment of the refugee camps.

In our study, we observed an average LST of approximately 31 °C in mixed forest areas, rising to 34 °C in built-up areas. The land area with an average temperature ranging from 30.5 to 33.5 °C has decreased from ~1493 hectares in 2013 to 122 hectares in 2024, which is very concerning, particularly if the situation continues. Similar results were also found

in other studies in Bangladesh. For instance, Ahmed et al. found that rapid urbanization in the Dhaka Metropolitan area significantly increased LST by replacing vegetation and water bodies with built-up areas, which expanded by 88.78% over 20 years (1989–2009). As a result, LST projections indicated that temperatures above 30 °C would affect 56% of the area by 2019 and 87% by 2029 [37].

Previous studies found that the anthropogenic degradation linked to the Rohingya refugee influx has exacerbated forest loss through two primary mechanisms. First, during the camp establishment in 2017, approximately 2500 hectares of predominantly natural and mixed forests were cleared to accommodate an estimated 750,000 refugees [38]. Second, both degraded and intact forests around the camps are frequently encroached upon by refugees for fuelwood collection, which is used for cooking or sold in local markets [14,39]. This extensive deforestation has also resulted in significant habitat loss in protected areas such as Teknaf Wildlife Sanctuary, Himchari National Park, and Inani National Park. Notably, Asian elephants, which are classified as endangered by the IUCN, have faced disruptions due to blocked migratory corridors and food scarcity, leading to human–elephant conflicts, with 13 fatalities and over 50 injuries reported between 2017 and 2019 [40,41]. Governmental authorities, NGOs, and international humanitarian organizations have initiated efforts to mitigate environmental degradation. Our study observed a 43% increase in green areas from 2018 to 2024, largely due to reforestation efforts led by UNHCR and its partners. Between 2018 and 2021, approximately 600 hectares of land were reforested with fast-growing native tree species, shrubs, and grasses [34].

These results highlight critical biome-societal feedback. While the establishment of refugee settlements provided immediate shelter, it also triggered cascading ecological consequences that, in turn, affected human well-being. Rising temperatures, reduced forest cover, and loss of water resources increase susceptibility to extreme weather events, diminish agricultural productivity, and contribute to deteriorating living conditions [9,14]. Notably, international and national interventions, such as tree planting initiatives and the introduction of liquefied petroleum gas (LPG) as an alternative to firewood, have contributed to modest improvements in environmental conditions, but they remain insufficient to counterbalance the scale of deforestation-induced thermal shifts [42,43].

Despite these positive interventions, our findings and similar studies indicate that LST has steadily increased. This can be attributed to several factors. First, newly planted vegetation may not yet be mature enough to provide substantial cooling effects [44]. Zhao et al. found that the cooling impact of vegetation intensifies as tree canopies develop and expand [45]. Second, while reforestation efforts have increased green cover, the significant expansion of built-up areas and reduction of natural forests have likely counterbalanced the cooling effects of afforestation [46]. Newly planted areas often lack mature forests' complex structure and evapotranspiration capacity, limiting their immediate impact on LST in a region still dominated by built-up surfaces and degraded forests. A comprehensive approach combining multiple strategies is essential to effectively mitigate urban heat. For instance, Zhao et al. proposed a whole system approach, highlighting the need for context-specific, multi-measure strategies to effectively mitigate urban heat [47]. It emphasizes that decision-making should focus on investment, time for implementation, and effectiveness. Kumar et al. explored how green–blue–gray infrastructures (GBGIs), such as parks, wetlands, and engineering greening, help mitigate urban heat. It provides a global inventory of 51 GBGI types, emphasizing the need for strategic implementation that maximizes cooling benefits while considering ecological, social, and policy factors [48]. Overall, strategic interventions, such as afforestation programs and sustainable land-use policies, have shown promise in reversing some of these trends. These global examples suggest that a combination of

targeted afforestation, improved urban planning, and climate-sensitive infrastructure could enhance resilience in Cox's Bazar as well.

Future studies should focus on quantifying the long-term climatic effects of refugee-induced deforestation and evaluating policy interventions aimed at restoring ecological stability. Moreover, a more detailed socio-environmental assessment incorporating community adaptation strategies would offer a holistic understanding of how displaced populations interact with and modify their surroundings over time [47,48].

5. Conclusions

This study provides robust evidence of the profound environmental consequences of forced displacement, demonstrating how the rapid expansion of the Rohingya refugee camps in Cox's Bazar has altered land cover patterns and exacerbated land surface temperature dynamics. A detailed analysis of the significant impacts of LULC changes on LST was conducted in the Rohingya refugee area of Cox's Bazar, Bangladesh, from 2013 to 2024. Our findings reveal a dramatic transformation in the landscape, driven largely by establishing and expanding refugee camps to accommodate over one million displaced individuals. Between 2013 and 2018, mixed forest areas experienced a drastic reduction of 97%, while built-up areas grew by 161.78%. This deforestation and urbanization have significantly increased LST, with the cooler zones shrinking to negligible levels and high-temperature zones expanding substantially. The correlation between LST and indices such as NDVI, NDWI, and NDBI highlights the role of vegetation and water bodies in regulating temperatures, whereas urbanization exacerbates the urban heat island effect.

The study also notes the positive but limited impact of reforestation efforts from 2018 to 2024, which resulted in a 43% increase in green areas. However, the immaturity of newly planted vegetation and the continued expansion of built-up zones have limited their cooling effects. The analysis underscores the urgent need to balance humanitarian needs with environmental preservation to prevent further ecosystem degradation in this vulnerable region. Mixed forest areas were identified as the most effective in reducing LST, emphasizing the critical role of green spaces in mitigating heat stress and stabilizing the local climate.

This study underscores the critical need for integrating environmental sustainability with humanitarian responses. International collaboration is vital for addressing long-term challenges. Efforts should include bilateral discussions between Bangladesh and Myanmar for the safe and dignified repatriation of refugees and global stakeholder support to share environmental and humanitarian burdens. Establishing continuous monitoring systems using satellite imagery and ground-based observations will allow for real-time assessment and adaptation of mitigation strategies. Combining sustainable policies, international cooperation, and community education can reduce environmental degradation, enhance climate resilience, and create a more sustainable future for refugees and host communities.

Further research is needed to model future climate scenarios under different land-use strategies and to explore innovative approaches [12]. A multidisciplinary approach combining remote sensing, field surveys, and policy analysis would provide deeper insights into the evolving relationship between refugee settlements and environmental change [47]. As forced displacement continues to shape landscapes worldwide, this study provides a crucial foundation for understanding how biome-societal feedback influences regional climate systems and how proactive planning can mitigate long-term ecological harm [46].

Lastly, we would like to mention several caveats associated with this study. While land surface temperatures are an important indicator of UHI, they alone cannot fully represent its complexity. Additional factors such as anthropogenic heat emissions, air circulation, humidity, and building density should be included to achieve a comprehensive

understanding. Another limitation of the study is that we could not identify the physical mechanisms underlying the impact of NDVI, NDWI, and NDBI on LST.

Author Contributions: Conceptualization and methods, S.K. and M.R.; formal analysis, S.K. and M.R.; data curation, S.K. and M.R.; writing-original draft preparation, S.K. and M.R.; writing-review and editing, L.M., S.K. and M.R.; visualization, S.K. and M.R.; supervision, L.M.; project administration, L.M.; funding acquisition, L.M. All authors have read and agreed to the published version of the manuscript.

Funding: L. Meng was partially funded by the Milton & Ruth Scherer Endowment Fund in the School of Environment, Geography, and Sustainability at Western Michigan University.

Institutional Review Board Statement: Not applicable.

Informed Consent Statement: Not applicable.

Data Availability Statement: The data presented in this study are available upon request from the corresponding author. The data are not publicly available due to privacy.

Conflicts of Interest: The authors declare no conflicts of interest.

Appendix A

Table A1. Satellite images used in this study.

Image ID	Date	Cloud Cover	Year
LC08_135045_20130414	2013-04-14	5.2	2013
LC08_135045_20130430	2013-04-30	12.8	2013
LC08_135046_20130414	2013-04-14	3.08	2013
LC08_135045_20180412	2018-04-12	2.58	2018
LC08_135045_20180428	2018-04-28	0.33	2018
LC08_135046_20180412	2018-04-12	0.82	2018
LC08_135046_20180428	2018-04-28	2.8	2018
LC08_136045_20180403	2018-04-03	2.3	2018
LC08_136046_20180403	2018-04-03	5.62	2018
LC08_136046_20180505	2018-05-05	19.25	2018
LC08_135045_20240428	2024-04-28	13.76	2024
LC08_135045_20240514	2024-05-14	5.43	2024
LC08_135046_20240412	2024-04-12	5.88	2024
LC08_135046_20240428	2024-04-28	11.25	2024
LC08_135046_20240514	2024-05-14	6.19	2024
LC08_136045_20240419	2024-04-19	13.77	2024
LC08_136046_20240403	2024-04-03	5.92	2024
LC08_136046_20240419	2024-04-19	7.6	2024
LC08_136046_20240521	2024-05-21	16.13	2024

Table A2. Calculated areas for different index ranges, presented in hectares (ha) and in % of the total study area.

Index	Area (ha)	Area (ha)	Area (ha)	Area (%)	Area (%)	Area (%)
LST Range	2013	2018	2024	2013	2018	2024
<30.5	41.58	0	4.41	1.56%	0.00%	0.17%
30.5–33.5	1493.46	53.01	121.68	56.08%	1.99%	4.57%
33.5–36.5	905.4	434.34	1187.46	34.00%	16.31%	44.59%
36.5–39.5	188.01	1094.94	1038.96	7.06%	41.12%	39.02%
>39.5	34.47	1083.63	310.41	1.29%	40.58%	11.66%
NDVI Range	2013	2018	2024	2013	2018	2024
<0.2	17.73	367.02	46.53	0.67%	13.78%	1.75%
0.2–0.4	148.77	1467.54	1102.59	5.58%	55.09%	41.39%
0.4–0.6	544.23	701.19	1314.72	20.43%	26.32%	49.35%
0.6–0.8	1420.74	128.16	200.07	53.33%	4.81%	7.51%
>0.8	532.44	0	0	19.99%	0%	0%
NDWI Range	2013	2018	2024	2013	2018	2024
<−0.08	4.86	82.08	60.75	0.18%	3.088%	2.289%
−0.08–0.06	200.7	1645.56	916.38	7.53%	61.778%	34.40%
0.06–0.21	644.76	758.07	1499.04	24.20%	28.46%	56.27%
0.21–0.35	1180.17	173.16	178.29	44.30%	6.50%	6.69%
>0.35	633.42	5.04	9.45	23.78%	0.19%	0.35%
NDBI Range	2013	2018	2024	2013	2018	2024
<−0.35	633.42	5.04	9.45	23.78%	0.19%	0.35%
−0.35–−0.2	1245.24	210.33	216.45	46.74%	7.9%	8.13%
−0.2–−0.05	606.15	790.65	1587.24	22.75%	29.68%	59.58%
−0.05–0.1	177.3	1626.66	816.3	6.66%	61.06%	30.64%
>0.1	1.8	31.23	34.47	0.07%	1.17%	1.29%

References

1. Zhu, Y.; Shi, Y. Spatio-temporal variations of PM2.5 concentrations and related premature deaths in Asia, Africa, and Europe from 2000 to 2018. *Environ. Impact Assess. Rev.* **2023**, *99*, 107046. [CrossRef]
2. Rohingya Refugee Crisis Explained. Available online: https://www.unrefugees.org/news/rohingya-refugee-crisis-explained/#RohingyainBangladesh (accessed on 16 December 2024).
3. Bakebillah, M.; Ahmad, M.M. *Half a Decade of the Rohingya Refugee Crisis: The Threats to Peace and Sustainability in Bangladesh*; Springer: Singapore, 2024; pp. 137–157. [CrossRef]
4. Obaidullah, M.; Hossain, M.; Raihan, S.; Hossen, S. From humanitarian crisis to burden: Understanding the Rohingya refugee crisis in Bangladesh. *SN Soc. Sci.* **2024**, *4*, 141. [CrossRef]
5. Nogbou, H.-A.; Nalugala, R. Ecosystem Sustainability for Improved Refugees' Livelihood: A Case of Kalobeyei Integrated Settlement, in Turkana County, Kenya. *Eur. J. Dev. Stud.* **2022**, *2*, 29–38. [CrossRef]
6. Rahman, M.; Islam; Chowdhury, T. Change of Vegetation Cover at Rohingya Refugee Occupied Areas in Cox's Bazar District of Bangladesh: Evidence from Remotely Sensed Data. *J. Environ. Sci. Nat. Resour.* **2019**, *11*, 9–16. [CrossRef]
7. Rahman, M.; Meng, L. Examining the Spatial and Temporal Variation of $PM_{2.5}$ and Its Linkage with Meteorological Conditions in Dhaka, Bangladesh. *Atmosphere* **2024**, *15*, 1426. [CrossRef]
8. Rahman, M.; Meng, L.; Mathews, A.J.; Bertman, S. Spatiotemporal Analysis of Urban Growth and $PM_{2.5}$ Concentrations in Sylhet, Bangladesh. *Atmosphere* **2024**, *15*, 1305. [CrossRef]

9. Imtiaz, S. Ecological impact of Rohingya refugees on forest resources: Remote sensing analysis of vegetation cover change in Teknaf Peninsula in Bangladesh. *Ecocycles* **2018**, *4*, 16–19. [CrossRef]
10. Hasan, M.E.; Zhang, L.; Dewan, A.; Guo, H.; Mahmood, R. Spatiotemporal pattern of forest degradation and loss of ecosystem function associated with Rohingya influx: A geospatial approach. *Land Degrad. Dev.* **2020**, *32*, 3666–3683. [CrossRef]
11. Ren, Y.; Lafortezza, R.; Giannico, V.; Sanesi, G.; Zhang, X.; Xu, C. The unrelenting global expansion of the urban heat island over the last century. *Sci. Total Environ.* **2023**, *880*, 163276. [CrossRef] [PubMed]
12. Al Kafy, A.; Dey, N.N.; Saha, M.; Altuwaijri, H.A.; Fattah, A.; Rahaman, Z.A.; Kalaivani, S.; Bakshi, A.; Rahaman, S.N. Leveraging machine learning algorithms in dynamic modeling of urban expansion, surface heat islands, and carbon storage for sustainable environmental management in coastal ecosystems. *J. Environ. Manag.* **2024**, *370*, 122427. [CrossRef] [PubMed]
13. Mahi, M.M.; Sharif, S.; Rudra, R.R.; Haque, N. THE geo-spatial approach to detect the change in vegetation and land surface temperature (LST) after formation of rohingya settlements in Bangladesh. *J. Civ. Eng. Sci. Technol.* **2021**, *12*, 229–242. [CrossRef]
14. Bappa, S.A.; Malaker, T.; Mia, R.; Islam, D. Spatio-temporal variation of land use and land cover changes and their impact on land surface temperature: A case of Kutupalong Refugee Camp, Bangladesh. *Heliyon* **2022**, *8*, e10449. [CrossRef] [PubMed]
15. Kudrat-E-Khuda (Babu). The impacts and challenges to host country Bangladesh due to sheltering the Rohingya refugees. *Cogent Soc. Sci.* **2020**, *6*, 1770943. [CrossRef]
16. Wang, L.; Lu, Y.; Yao, Y. Comparison of Three Algorithms for the Retrieval of Land Surface Temperature from Landsat 8 Images. *Sensors* **2019**, *19*, 5049. [CrossRef]
17. Jimenez-Munoz, J.C.; Sobrino, J.A. A Single-Channel Algorithm for Land-Surface Temperature Retrieval from ASTER Data. *IEEE Geosci. Remote Sens. Lett.* **2010**, *7*, 176–179. [CrossRef]
18. Vermote, E.; Justice, C.; Claverie, M.; Franch, B. Preliminary analysis of the performance of the Landsat 8/OLI land surface reflectance product. *Remote Sens. Environ.* **2016**, *185*, 46–56. [CrossRef]
19. Mountrakis, G.; Im, J.; Ogole, C. Support vector machines in remote sensing: A review. *ISPRS J. Photogramm. Remote Sens.* **2011**, *66*, 247–259. [CrossRef]
20. Pal, M.; Mather, P.M. Support vector machines for classification in remote sensing. *Int. J. Remote Sens.* **2005**, *26*, 1007–1011. [CrossRef]
21. Foody, G.M. Status of land cover classification accuracy assessment. *Remote Sens. Environ.* **2002**, *80*, 185–201. [CrossRef]
22. Guha, S.; Govil, H. Annual assessment on the relationship between land surface temperature and six remote sensing indices using landsat data from 1988 to 2019. *Geocarto Int.* **2022**, *37*, 4292–4311. [CrossRef]
23. Hasan, M. Spatio-Temporal Analysis of Cox's Bazar from 1990 to 2020: Exploring the Relationship between LST, NDVI, NDBI and LULC. *Res. Sq.* **2024**. [CrossRef]
24. Al Kafy, A.; Rahman, S.; Faisal, A.-A.; Hasan, M.M.; Islam, M. Modelling future land use land cover changes and their impacts on land surface temperatures in Rajshahi, Bangladesh. *Remote Sens. Appl.* **2020**, *18*, 100314. [CrossRef]
25. Lo, C.P.; Quattrochi, D.A.; Luvall, J.C. Application of high-resolution thermal infrared remote sensing and GIS to assess the urban heat island effect. *Int. J. Remote Sens.* **1997**, *18*, 287–304. [CrossRef]
26. Wang, G.; Tian, G.; Jombach, S.; Li, H. Mapping and Analyzing the Park Cooling Effect on Urban Heat Island in an Expanding City: A Case Study in Zhengzhou City, China. *Land* **2020**, *9*, 57. [CrossRef]
27. Guha, S.; Govil, H.; Besoya, M. An investigation on seasonal variability between LST and NDWI in an urban environment using Landsat satellite data. *Geomat. Nat. Hazards Risk* **2020**, *11*, 1319–1345. [CrossRef]
28. Varshney, A. Improved NDBI differencing algorithm for built-up regions change detection from remote-sensing data: An automated approach. *Remote Sens. Lett.* **2013**, *4*, 504–512. [CrossRef]
29. Lu, D.; Song, K.; Zang, S.; Jia, M.; Du, J.; Ren, C. The Effect of Urban Expansion on Urban Surface Temperature in Shenyang, China: An Analysis with Landsat Imagery. *Environ. Model. Assess.* **2015**, *20*, 197–210. [CrossRef]
30. Tucker, C.J. Red and photographic infrared linear combinations for monitoring vegetation. *Remote Sens. Environ.* **1978**, *8*, 127–150. [CrossRef]
31. McFeeters, S.K. The use of the Normalized Difference Water Index (NDWI) in the delineation of open water features. *Int. J. Remote Sens.* **1996**, *17*, 1425–1432. [CrossRef]
32. Zha, Y.; Gao, J.; Ni, S. Use of normalized difference built-up index in automatically mapping urban areas from TM imagery. *Int. J. Remote Sens.* **2003**, *24*, 583–594. [CrossRef]
33. Yasmin, T.; Dhesi, S.; Kuznetsova, I.; Cooper, R.; Krause, S.; Lynch, I. A system approach to water, sanitation, and hygiene resilience and sustainability in refugee communities. *Int. J. Water Resour. Dev.* **2023**, *39*, 691–723. [CrossRef]
34. UNHCR. Rohingya Refugees Restore Depleted Forest in Bangladesh. Available online: https://www.unhcr.org/news/stories/rohingya-refugees-restore-depleted-forest-bangladesh (accessed on 21 November 2024).
35. Rashid, K.J.; Hoque, A.; Esha, T.A.; Rahman, A.; Paul, A. Spatiotemporal changes of vegetation and land surface temperature in the refugee camps and its surrounding areas of Bangladesh after the Rohingya influx from Myanmar. *Environ. Dev. Sustain.* **2021**, *23*, 3562–3577. [CrossRef]

36. Yaseen, A.; Khan, A. Monitoring The Land Surface Temperature and Its Correlation with NDVI of Chiniot by Using GIS Technology and Remote Sensing. *J. Earth Sci. Clim. Change* **2022**, *13*, 621. [CrossRef]
37. Ahmed, B.; Kamruzzaman, M.; Zhu, X.; Rahman, M.S.; Choi, K. Simulating land cover changes and their impacts on land surface temperature in Dhaka, Bangladesh. *Remote Sens.* **2013**, *5*, 5969–5998. [CrossRef]
38. Sarkar, S.K.; Saroar, M.; Chakraborty, T. Navigating nature's toll: Assessing the ecological impact of the refugee crisis in Cox's Bazar, Bangladesh. *Heliyon* **2023**, *9*, e18255. [CrossRef]
39. Tani, M.; Rahman, M.A. *Deforestation in the Teknaf Peninsula of Bangladesh: A Study of Political Ecology*; Springer: Singapore, 2017; pp. 1–204. [CrossRef]
40. UNHCR. IUCN Launch Plan to Prevent Human-Elephant Conflict in Bangladesh Refugee Settlement | IUCN. Available online: https://iucn.org/news/bangladesh/201803/unhcr-iucn-launch-plan-prevent-human-elephant-conflict-bangladesh-refugee-settlement (accessed on 21 November 2024).
41. MRahman, H. Rohingya refugee crisis and human vs. elephant (Elephas maximus) conflicts in Cox's Bazar district of Bangladesh. *J. Wildl. Biodivers.* **2019**, *3*, 10–21. [CrossRef]
42. Sarkar, S.K.; Saroar, M.; Chakraborty, T. Cost of Ecosystem Service Value Due to Rohingya Refugee Influx in Bangladesh. *Disaster Med. Public Health Prep.* **2023**, *17*, e198. [CrossRef]
43. Sultana, Z. Impact of Rohingya influx on host community's relations to places in Bangladesh. *Int. J. Intercult. Relat.* **2023**, *93*, 101782. [CrossRef]
44. Ahmed, F.; Alam, S.; Saha, O.R.; Rahman, A. The Rohingya refugee crisis in Bangladesh: Assessing the impact on land use patterns and land surface temperature using machine learning. *Environ. Monit. Assess.* **2024**, *196*, 555. [CrossRef]
45. Zhao, L.; Lee, X.; Smith, R.B.; Oleson, K. Strong contributions of local background climate to urban heat islands. *Nature* **2014**, *511*, 216–219. [CrossRef]
46. Li, X.; Zhou, Y.; Asrar, G.R.; Imhoff, M.; Li, X. The surface urban heat island response to urban expansion: A panel analysis for the conterminous United States. *Sci. Total Environ.* **2017**, *605–606*, 426–435. [CrossRef] [PubMed]
47. Zhao, Y.; Sen, S.; Susca, T.; Iaria, J.; Kubilay, A.; Gunawardena, K.; Zhou, X.; Takane, Y.; Park, Y.; Wang, X.; et al. Beating urban heat: Multimeasure-centric solution sets and a complementary framework for decision-making. *Renew. Sustain. Energy Rev.* **2023**, *186*, 113668. [CrossRef]
48. Kumar, P.; Debele, S.E.; Khalili, S.; Halios, C.H.; Sahani, J.; Aghamohammadi, N.; Andrade, M.d.F.; Athanassiadou, M.; Bhui, K.; Calvillo, N.; et al. Urban heat mitigation by green and blue infrastructure: Drivers, effectiveness, and future needs. *Innovation* **2024**, *5*, 100588. [CrossRef] [PubMed]